γ-ray spectroscopy with a LaBr(Ce) scintillation detector at ultra high count rates

γ-Spektroskopie mit einem LaBr(Ce) Szintillationsdetektor bei sehr hohen Zählraten

Project-Proposal von Bastian Löher

April 2010

TECHNISCHE UNIVERSITÄT DARMSTADT

SFB 634

γ-ray spectroscopy with a LaBr(Ce) scintillation detector at ultra high count rates
γ-Spektroskopie mit einem LaBr(Ce) Szintillationsdetektor bei sehr hohen Zählraten

Vorgelegtes Project-Proposal von Bastian Löher

1. Gutachten: Prof. Dr. Norbert Pietralla
2. Gutachten: Dr. Deniz Savran

Tag der Einreichung:

Abstract

This thesis proposal concerns the evaluation of a fast pile-up correction algorithm for application on detector pulses from an LaBr(Ce) scintillation detector. At ultra high count rates beyond the kBq regime pile-up correction becomes necessary even for such a fast scintillator. The correction method is assessed in a set of tests using digital traces comprised of carefully modeled synthetic signals. It is also applied to preliminary data from a ^{137}Cs source recorded with a 2 GHz flash ADC. For data acquisition and analysis several tools have been developed and are presented. The main work units for the course of the Master Thesis are proposed including a preliminary schedule.

Contents

1 Introduction

γ-ray spectroscopy has been one of the preferred tools in nuclear physics to determine important properties of nuclei. Ever since their invention scintillation detectors and semiconductor detectors have become more and more powerful devices to probe the internal structure of thousands of different isotopes by detecting the emitted γ-rays originating from radioactive decay. Within this proposal I would like to focus on a specific limitation which does not only apply to γ-ray detectors, but which does affect particle detectors in general. However due to its special application at the photon tagger NEPTUN [Sav10] this proposal is mainly geared towards γ-ray spectroscopy. In chapter 1 I am going to stress the importance of resolving the issue of pile-up events in γ-ray detectors at high count rates, and why this is important for the course of my Master Thesis. With this in mind I want to propose in chapter 2 a fast method for correcting pile-up events using digital data acquisition and digital signal processing methods, which can be applied to signals from Lanthanum Bromide (LaBr(Ce)) scintillation detectors. I will also test this method with a number of simulated synthetic signals, in order to obtain optimal values for the algorithm parameters. Chapter 3 will mainly focus on the computational tools I have developed in the course of my studies. I will give a short overview of the scope software for data acquisition and the structure of the C++ library *SamDSP* for digital signal processing (DSP). In chapter 4 I will present the future plans for my master's thesis, which include the test and commissioning of the new LaBr(Ce) detector, the investigation of several important detector properties, and the design and construction of an active beam dump at the low energy photon tagger NEPTUN at the super conducting linear accelerator S-DALINAC [Ric96] at the TU Darmstadt. The proposed active beam dump will allow the determination of important experimental properties like the tagged photon energy and the absolute photon flux.

1.1 Motivation

Since radioactive decay can happen at immense rates, either because the source activity is extremely high or because of an intense beam at an accelerator facility, the detector system for the decay products must be able to cope with these high rates. If the decay rate is higher than the detection capability of the detector system, then the detection efficiency of the system decreases. At first glance this circumstance might not seem like a serious issue at all. Indeed in many cases directly addressing this issue has been avoided using a variety of workaround measures.

Dead time

To understand why a detector system has a limited detection rate one has to introduce the concept of *dead time*. This is the period of time from the first interaction of the particle with the sensitive medium until the detector has returned to its initial state. Usually during this time the detector is blind for any additional events. To avoid confusion I would like to clarify that throughout this proposal the term *dead time* always refers to the intrinsic dead time of the detector system, not to dead time introduced by the limited processing capability of the data acquisition system. Depending on the detector system the dead time can be in the range of many *ns* to a few *ms*, limiting the detection rate to a maximum of a few MHz. One of the most often used detectors for high resolution γ-ray spectroscopy are high purity germanium (HPGe) detectors, because of its very good intrinsic resolution of better than 2 keV at 1.33 MeV photon energy. Due to the charge collection mechanism involved, these detectors generate relatively slow signals which results in longer dead times. As already stated above, this leads to a limited detection rate, which affects a wide variety of experiments in nuclear physics. Also scintillation detectors such as NaI or CsI crystals are commonly used in γ-ray spectroscopy, but are either limited in resolution or produce similarly slow signals. To comply with this limitation, often the beam intensity has to be lowered, the radioactive source or target has to be measured in a different geometry, or other compromises have to be made by the experimentalists. In order to overcome or at least soften this dead time limitation one has to take a closer look at the cause of dead time.

Pile-Up

From this point on I would like to focus mainly on scintillation detectors. In most cases the ultimate cause of dead time in detector systems is the fact that each generated signal has a finite length, as can be seen in figure 1.1. This length is determined by a number of factors, most of which depend on the detector material, the detector geometry, and also the front end electronics. Usually for a given experiment all of these factors should have been considered and optimized, so that the signal length already is at a minimum. Two events occurring in a detector in this experiment can only be processed, if they are separated by at least this signal length, otherwise the signals would start to overlap. This case is shown in figure 1.2, where two ideal signals overlap, because their length is larger than their separation in time. A

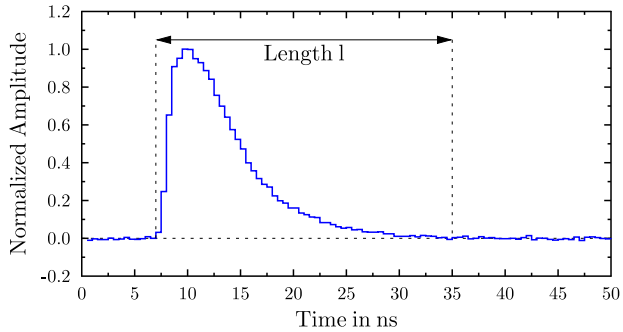

Figure 1.1: A single digitized signal from a scintillation detector. The finite length l is a characteristic property of the scintillation material.

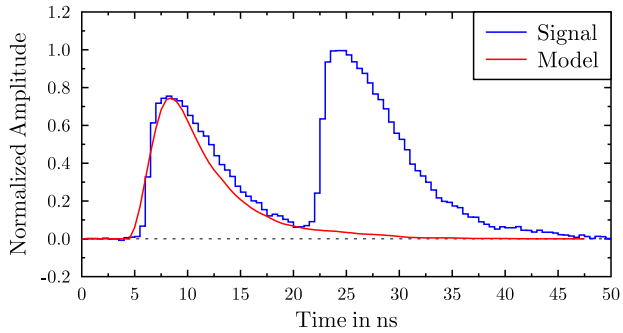

Figure 1.2: Example of two piled up signals. A model pulse (red) is shown on top of the first signal. Since the time difference between the two signals is small enough, the tail of the first signal contributes to the amplitude of the second signal. This leads to measurement errors.

situation like this is often referred to as *pile-up*. In γ-ray spectroscopy the most important information conveyed by a detected signal is its representation of the energy that a photon has deposited in the sensitive medium. This information can usually be determined by measuring the collected charge, or if the shape of the signal is constant, by measuring the amplitude of the signal. In a pile-up situation, this information is not as easy to determine. As the figure shows, neither the amplitude of nor the area under the second signal are directly accessible properties. The attempt to measure these properties regardless of the situation would result in values larger than the true values, which would then contribute to higher energies in a spectrum. The energy resolution as well as the efficiency of the detector would be reduced.

Pile-Up Rejection

If the detector has successfully detected an event, the probability that no additional events occur in a small time period τ after a detected event is given by

$$P(0) = e^{-n\tau}, \tag{1.1}$$

where n is the actual event rate [Kno00]. If τ is the dead time of the detector system, it is clear that for low event rates almost all events can be detected. The probability of a piled up event to take place is rather low and using analog electronics, these events can be identified and suppressed, so that they do not contribute to the energy spectrum. This so called pile-up rejection mechanism maintains the energy resolution of the spectrum by sacrificing detector efficiency. The probability for piled up events as a function of the number of signals N occurring in the time period τ is given by

$$P(N) = \frac{(n\tau)^N e^{-n\tau}}{N!}. \tag{1.2}$$

This relation is visualized in figure 1.3, where on the left pane the probability $P(N)$ is plotted for several values of N over the product of count rate n and interval size τ. With increasing event rates the probability for piled up events with $N > 0$ increases, until the probability for single events ($N = 0$) is comparably low. The right pane shows the accumulated probabilities, and one can see that the fraction of single events drops below 10% when $n\tau > 2$. The pile-up rejection mechanism is in this case useless, because the efficiency would tend to zero.

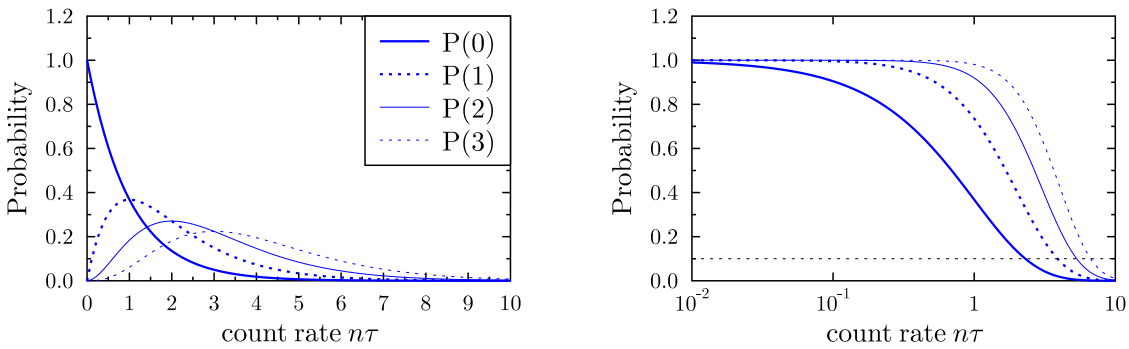

Figure 1.3: *Left*: Probabilty $P(N)$ of detecting N signals within the time interval τ at a count rate of n for several values of N. *Right*: Accumulated probabilites. For count rates around $n\tau = 2$ the probability for detecting a single signal drops below 10 %. In this regime pile-up rejection is no longer feasible.

New approaches

In the recent past there have been many attempts to address the issue of pile-up with a variety of methods. For large HPGe detectors a method using a time-domain Moving Window Deconvolution has been developed [Geo93], but it is difficult to apply to very short signals. If the detector signal dynamics can be expressed with a mathematical model, then Kalman smoothing can be applied, as is presented in [Bar06] for HPGe detectors. For $LaCl_3$ another deconvolution method has been developed in which first the detector system response function is determined and then the deconvolution is done in the frequency domain [Yan09]. Also computationally intensive methods such as pulse fitting methods (e.g. [Bel08]) have already been presented. In this proposal I am going to show the applicability of a fast digital pile-up reconstruction algorithm, which takes ordinary listmode data as input and performs the reconstruction using a matrix inversion. The method has originally been developed for pile-up correction of NaI detector pulses [Ven09]. The input listmode data for the algorithm is produced from digitized detector signals.

1.2 Application at NEPTUN

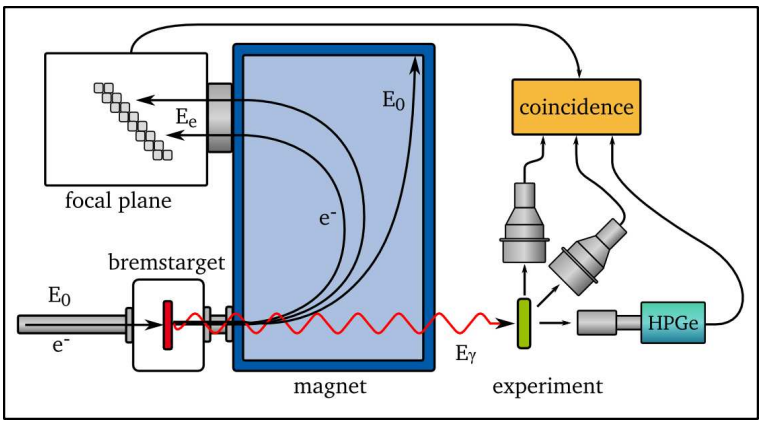

Figure 1.4: Schematic drawing of the NEPTUN tagger experimental setup. An incident electron beam creates bremsstrahlung photons in the bremstarget. The scattered electrons are analysed with a dipole magnet and detected in the segmented focal plane. With a coincidence unit each produced photon can be assigned to a scattered electron, and thus the photon energy can be determined.

The low energy photon tagger NEPTUN is designed to produce photons in the range of 3 to 15 MeV with an energy uncertainty of about 35 keV at 10 MeV for nuclear structure and nuclear astrophysics experiments. The photons are produced as bremsstrahlung radiation from a radiator target, and their energy is determined by measuring the energy loss of the scattered electrons with a dipole magnet. Using the coincidence between the detection of the bremsstrahlung photon and the scattered electron in the segmented focal plane of the magnet it is possible to assign a photon to a

scattered electron. It is necessary to precisely know the energy and its temporal stability, which is tagged with a specific setting of the magnetic field of the dipole magnet. This can be done with a high resolution γ-ray detector set directly in-beam behind the experiment, as sketched in figure 1.4. With an HPGe detector the energy can only be determined when the beam intensity is low, compared to an actual experiment, in order to avoid driving the detector into pile-up. This procedure reduces the amount of time available for experiments and requires frequent changes in the geometrical setup. Also data analysis can only be done offline, which limits feedback for the experimentalist. If instead a Lanthanum Bromide scintillation detector, which produces significantly shorter signals, is used, then it should be possible to maintain a high beam intensity while simultaneously monitoring the tagged beam energy. Measurement of the absolute photon flux might also be possible, if all single events can be resolved by the signal processing unit. These measurements can be done online, while the experiment is in progress, so that low latency feedback is available. Finally no unnecessary changes to the setup have to be done during an experiment and no time is lost for calibration measurements.

2 Lanthanum Bromide at high count rates

I want to begin this chapter with a motivation why Lanthanum Bromide has been chosen as the detector material even though there are many other materials available and why it is an excellent material for γ-ray spectroscopy in very high count rate applications. The main part of this chapter will focus on the digital pile-up correction algorithm to compensate the losses in efficiency and energy resolution due to pile-up. The algorithm will be tested with a range of synthetic simulated signals and traces in order to find the optimum parameters. The last part of this chapter will show some preliminary results produced with a test setup and a small detector.

2.1 Lanthanum Bromide as a fast scintillator

In the scope of this thesis proposal all data regarding Lanthanum Bromide Scintillators is taken from the Saint Gobain Data Sheets [StG08] for the BrilLanCe 380 crystal, because future studies will be carried out using a detector made from this material. Lanthanum Bromide ($LaBr_3$) is one of the scintillation materials from the range of Lanthanum Halides (LaX). It was invented in 2001 by the Delft University in The Netherlands, so it is still a considerably new material. Usually during production LaBr it is doped with Cerium to increase the light yield. In this configuration $LaBr_3$:Ce has a light yield of 63 photons per keV and incident γ-ray. This corresponds to about 165 % of the light yield of NaI(Tl). Light yield is one very important property for spectrometric applications, because if more photons are produced in the scintillator, the statistical error in the resulting signal decreases, which improves the resolution. The data sheet lists a resolution of less than 3.0 % for γ-rays at an energy of 662 keV from a ^{137}Cs source. NaI(Tl) detectors usually reach a resolution of about 7.0 % in this energy range. The second most important property of Lanthanum Bromide which is of advantage in high rate applications is the very low decay constant of 16 ns of the emitted light, which leads to very short signals. This allows very precise timing in the range of 300 ps using a specialized photomultiplier, or 400 ps with a standard PMT [StG09]. I will show in the next section that this precision timing is necessary for the pile-up correction algorithm to work properly. The fact that the signals are so short makes it possible to use a LaBr scintillation detector already at detection rates of up to 1 MBq without any treatment of pile-up. High Purity Germanium detectors instead usually saturate at detection rates of below 100 kBq. Hence their by far superior energy resolution can unfortunately not be used in high rate applications. Another nice feature of LaBr is its temperature stability and linearity. Over a range of 0 °C to 55 °C the amount of light output varies only slightly within 1 % [StG09]. One fact that I will only remark for completeness rather than importance for the rest of this proposal is that LaBr is itself radioactive and will decay with γ-ray energies of 32 keV and 1.5 MeV. In a 3 in by 3 in sized LaBr crystal the activity is about 200 Bq [Men06]. This activity can be substantial when measuring weak sources, but can be neglected in high count rate applications. In summary, if energy resolution is not the most important property to measure, then LaBr scintillation detectors are an excellent choice regarding light yield, timing properties, linearity and temperature stability.

2.2 Pile-Up Correction algorithm

For event rates of $n\tau > 1$, the detector is driven into pile-up and the detection rate (rate of correctly detected pulses) does not increase proportionally anymore. As discussed before this leads to a decrease in detector and photo peak efficiency and a loss of detector resolution. The pile-up rejection algorithm is not a feasible approach, because it is not possible to recover detector efficiency with this technique. Instead the application of a digital pile-up correction algorithm is proposed, which would allow the detector to be used at exceedingly high event rates, without as much sacrifice in photo peak efficiency or energy resolution. This algorithm has been developed by M. Vencelj *et. al.* as shown in [Ven09]. The applied method acts on basic listmode data consisting of timestamps and corresponding measured signal amplitudes. It is therefore necessary to first extract these listmode data from the digitized or simulated signals in a separate process. This is done by applying different digital filters to the signals and extracting time and amplitude information from the filtered products. The choice and parameterisation of each digital filter depends on the pulse shape of the signal and also on the noise level in the recorded signals.

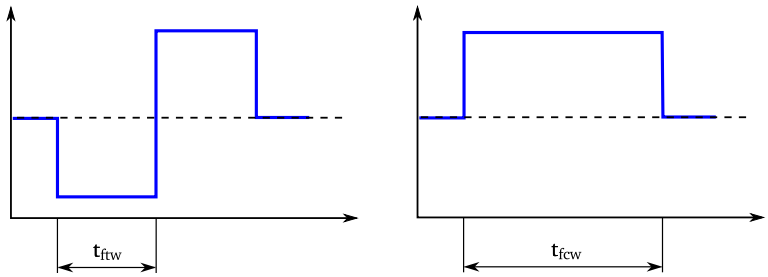

Figure 2.1: *Left*: Bibox FIR filter with duration $2t_{\mathrm{ftw}}$ for timing filtering. *Right*: Boxcar FIR filter with duration t_{fcw} for calorimetry.

2.2.1 Digital filtering

Fast digital filtering of time discrete signals is usually done by applying a time discrete convolution of the form

$$(f * g)[n] \stackrel{\text{def}}{=} \sum_{m=-\infty}^{\infty} f[n-m]\, g[m], \tag{2.1}$$

where the function f is convolved with the convolution kernel g. In the context of digital signal processing this convolution equation is often reduced to the so called finite impulse response (FIR) filtering, where the filter product

$$y[n] = \sum_{i=0}^{N} h_i\, x[n-i], \tag{2.2}$$

only depends on past values of the input signal x. The filter kernel coefficients h_i describe the weight with which each previous signal value contributes to the current output value. Usually N is much smaller than the amount of data points in the input signal. For the course of this proposal the two most important FIR filters are the boxcar filter and the bibox filter shown in figure 2.1. The boxcar filter is a simple integration filter and the output is comparable to a moving average, while the bibox filter is of a bipolar nature and serves as a differentiation filter. When the filters are applied to the input signal, not only the shape of the signal is altered accordingly, but also the signal amplitude changes and it is delayed in time. The effects of the different filters depend strongly on their widths , because the width of the filter determines how many data points are taken into account for calculating the output value. If a wider filter is used, then the signal is averaged over more data points, which leads to a reduction of noise in the signal. Thus each of these filters also act as a low pass filter on the signal. Whenever electronic signals are handled, the input signal usually is superimposed with a noise component. The effect of this noise, which is especially noticeable when the signal to noise ratio is relatively low, is to increase the timing and amplitude uncertainty of the signal. This effect will be discussed in the next section in more detail. In order to get the best results, the amount of noise in the signals has to be taken into account. Therefore the preparation of the signals prior to extracting useful information has to be investigated and the parameters have to be carefully adjusted.

2.2.2 Triggering

Digital triggering can be done in various ways, but in the frame of this proposal I would like to stick with the simple, yet powerful, method of filtering the signal with a bipolar FIR filter. Due to its local nature this method is also applicable in dense pile-up situations, as opposed to digital CFD or LED methods. The effect of this timing filter is shown in figure 2.2. It is obvious that the resulting signal has a much faster rise time than the original signal, so that timing measurement on this signal is more precise. The trigger signal is constructed by applying a trigger condition to the timing signal. A simple but fairly accurate trigger condition is to look for local maxima in the signal while the signal is above a certain threshold a_{thr}. The resulting trigger signal can then be used to measure the signal amplitude.

2.2.3 Digital calorimetry

In digital calorimetry of very fast signals it is important to integrate the signal over a certain range in order to measure a stable amplitude. If instead simply the peak point of the signal is used, then the resulting amplitude is more influenced by noise dependent fluctuations. These fluctuations can be reduced to a minimum, if the signal is filtered with an integrating

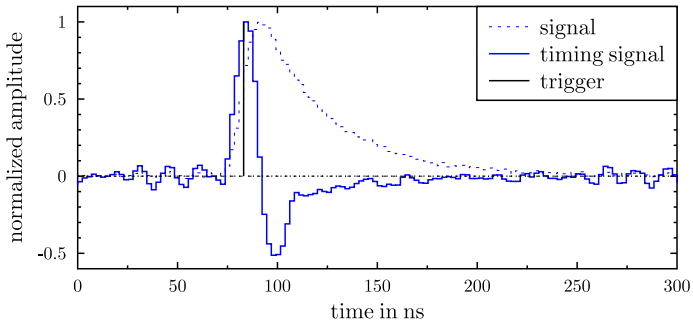

Figure 2.2: After filtering with a bibox filter, the signal (dashed line) is transformed into a much faster timing signal (solid line). With an appropriate trigger condition the trigger signal (black) is generated.

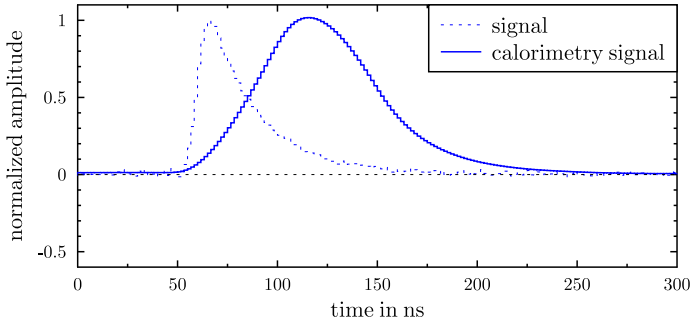

Figure 2.3: After filtering with an integrating box filter, the signal (dashed line) is transformed into a calorimetry signal (solid line) with a stable amplitude.

boxcar filter. The use of this filter smoothes the signal and reduces the noise component, as can be seen in figure 2.3. It is possible, that signals with a very small distance in time become indistinguishable after the filter has been applied. As stated before also the produced calorimetry signal is delayed in time by a constant value. In order to measure the amplitudes of the signals at the trigger positions this delay has to be compensated. This is done by simply applying each filter to a single signal and measuring the corresponding time shifts. The trigger signal and the calorimetry signal can be realigned and the signal amplitudes can be measured at the trigger positions. Of course these measured amplitudes are only correct, if none of the signals overlap. In case of pile-up the measured amplitudes have to be corrected.

2.2.4 Pile-Up Correction

Whenever two or more pulses occur close together in time and overlap partially, the measured amplitudes no longer reflect the true amplitudes of the constituent signals, since their integrals overlap. This situation is demonstrated in figure 2.4, where as an example a group of five signals is shown. It is clear, that the measured amplitudes b_i do not correspond to the true amplitudes. The pile-up correction method is based on the fact, that the piled-up trace is a superposition of all signal pulses, and thus also the measured amplitude can be expressed as a linear combination of the true amplitudes of the constituent signals:

$$b_i = \sum_j m_{ij} a_i. \tag{2.3}$$

Of course this description is only valid, if the pulse shape is constant. The coefficients m_{ij} depend on the time difference of the ith pulse to all neighboring pulses and express the relative contribution of the jth pulse to the ith pulse. At this point it is already obvious, that a precise timing is mandatory for the actual process of resolving piled-up events. Small changes in the timestamp can already lead to significant changes in the contribution coefficient. Also if the trigger can not distinguish between two consecutive signals, then the pile-up correction algorithm acts as if only one signal is present and the amplitudes can not be corrected. As will be discussed in the next section this is especially noticeable for small signals which are very close to large signals.

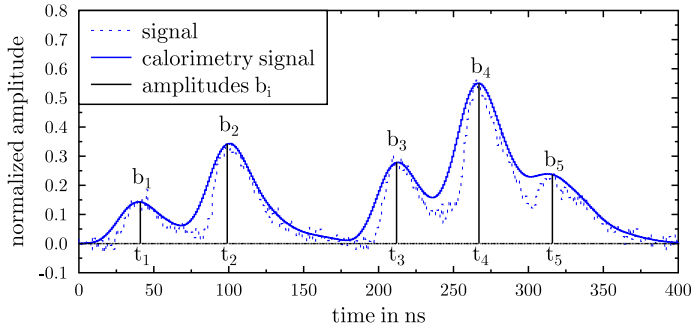

Figure 2.4: Example of a pile-up situation. Amplitudes (black) have been measured from the calorimetry filtered signal (solid line).

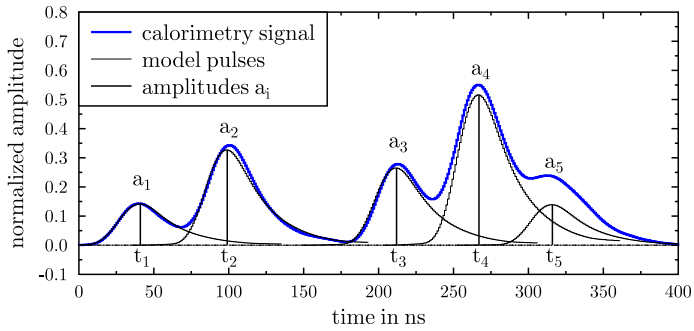

Figure 2.5: After pile-up correction the measured amplitudes b_i are corrected to yield the true amplitudes a_i (black). It is clear, that the superposition of the model pulse shapes (thin lines) results in the filtered signal (thick line).

The pile-up correction algorithm takes as input two vectors which contain both the timestamps t_i and the measured amplitudes b_i. The third and most important input for the algorithm is an accurate model pulse shape m of the signals which are to be measured. This model pulse shape can either be a numerical approximation of the real signal, or an average signal derived from measured signals at a low count rate setting. In any case the model pulse shape must be amplitude normalized, so that the peak data point has the value 1.0. From this model pulse shape the contribution coefficients m_{ij} are determined. Consider again the example from figure 2.4, then the amplitude of the rightmost signal (b_5) is enhanced by contributions of the two earlier signals. The relative amount of these contributions can be determined by superimposing the model pulse shape m at the timestamp of each contributing signal (here t_3, t_4) and measuring its value at timestamp t_5. So in general m_{ij} is given by the value of the model pulse shape at the time $t_{\max} + t_i - t_j$, where $t_{\max}$ is the time of the peak point in the model pulse shape. Even though it is possible to take into account the contributions of all other signals, it is advised to restrict the amount of neighboring signals considered to a small integer number in order to keep the computational effort low. To estimate a reasonable number of neighbors for a given count rate, the left part of figure 1.3 can be used. If all coefficients have been determined they can be combined into a square matrix $\mathbf{M}$, and eq. 2.3 can be written as

$$\mathbf{b} = \mathbf{M}\,\mathbf{a}. \tag{2.4}$$

The inverse of $\mathbf{M}$ can be calculated, but it has to be taken into account that $\mathbf{M}$ might be singular. With the inverse of $\mathbf{M}$ eq. 2.4 becomes

$$\mathbf{a} = \mathbf{M}^{-1}\,\mathbf{b}, \tag{2.5}$$

and the true amplitudes a_i can be calculated simply by multiplying the measured amplitudes b_i with $\mathbf{M}^{-1}$. If done right, the measured amplitudes are corrected and the trace is properly pile-up corrected, as can be seen in figure 2.5.

A number of free parameters control the behavior of the algorithm and the quality of the results. These parameters are the trigger filter width t_{ftw}, the trigger threshold a_{thr}, the calorimetry filter width t_{fcw}, and the number of signals N_{s} which are taken into account for each matrix inversion. This number also define the dimension $D = 2N_{\mathrm{s}} + 1$ of the matrix. The free parameters always have to be chosen in an optimal range to yield the best results in any possible pile-up situation.

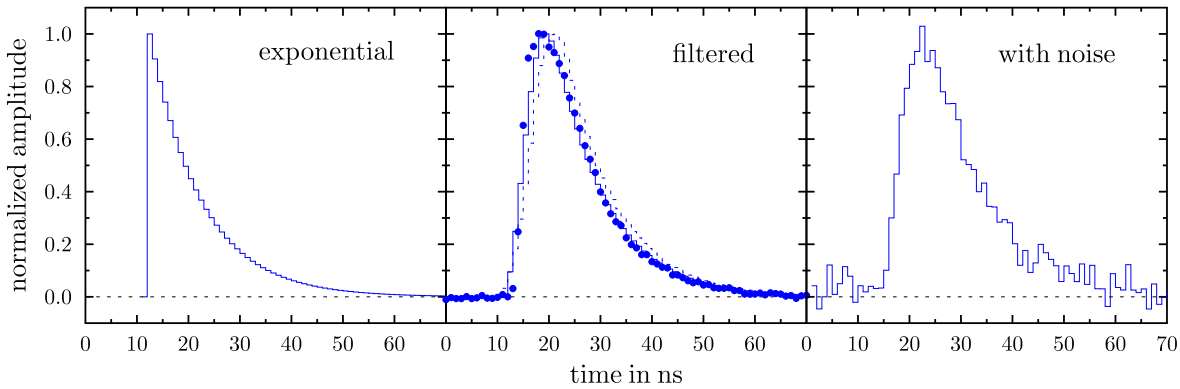

Figure 2.6: Composition of the simulated signal. *Left*: Simple exponential pulse with time constant $\tau = 16\,ns$. *Middle*: Dashed (solid) line: Exponential signal filtered with boxcar (ramp) filter. *Right*: Filtered signal with additional noise.

2.3 Application to simulated signals

In the following section the behavior and quality of the pile-up correction algorithm is investigated under variation of the free parameters and the pile-up situation. This is done using simulated signals, which are carefully modeled after the shape of real pulses and then combined into test cases. The advantage of this method is, that the result of the analysis is already known, and can be used to quantify the accuracy of the actual results. It is also possible to systematically create a range of test situations from a set of free parameters, which would not be possible in a real test setup.

2.3.1 Composition of realistic signals

At first it is important to mimic the shape of the expected detector signal as closely as possible, to maximize the applicability of the results. This can either be done by averaging over some recorded real signals, or by constructing the signal from components. The latter method has the advantage that the effect of each component can be investigated separately. In [Ben74] a formula is given to reproduce a scintillator pulse shape using a convolution of a gaussian with an exponential decay. This description makes the assumption that effects of the statistical scintillation process are negligible for large signals, and that all other statistical processes like electron emission on the photo cathode and production of secondary electrons in the photo multiplier can be described by the convolution with a gaussian. For the investigation of the best choice of parameters the simulated signals have been constructed in the following way:

Exponential decay

The first approximation of the scintillation signal is to use a simple exponential decay with the decay constant τ of the scintillator, shown in the left pane of figure 2.6. The decay constant is in this case $\tau = 16\,ns$. For detector signals which have a very short rise time compared to the decay constant this would already be a satisfying model. However, for LaBr signals this is not the case.

Filtered exponential

To mimic the statistical processes an FIR filter is applied. This adds a finite rise time to the signal. The middle pane of figure 2.6 shows this effect for two different filters in comparison to an actual detector signal. Displayed with a dashed line is the boxcar filter, which broadens the peak a lot. In order to resemble the actual signal more closely, a ramp filter (solid line) is used to produce a narrower peak. This was done as an approximation to [Ben78], where a clipped Gaussian is used as a filter to simulate ultra fast scintillator signals. The resulting rise time after filtering is about 8 ns.

Noise

Several sources of noise (electronic, statistical fluctuations) are combined into one white noise signal, which is superimposed on the filtered signal. The resulting signal is shown in the right pane of figure 2.6 and it seems valid to use the constructed signal as a good model pulse. The signal to noise ratio (SNR) is maintained as a free parameter for creating the simulated signals.

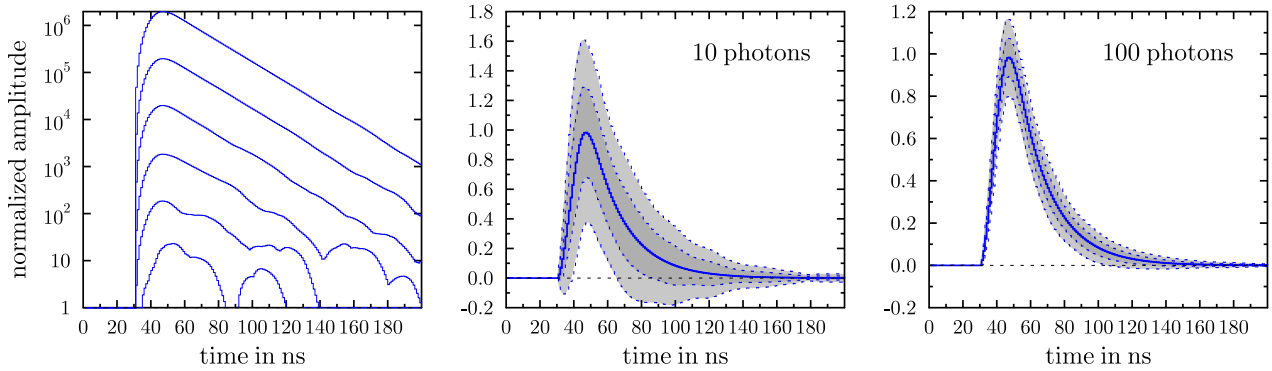

Figure 2.7: Photon statistics. *Left*: Filtered pulses generated with several amounts of photons ranging from 10^1 to 10^6. *Middle*: Single signal generated from 10 photons with 1σ and 2σ uncertainty intervals. *Right*: Same as in the middle, but with 100 photons. With increasing photon count signal uncertainties decrease, while at the start of a signal the uncertainty is always at a minimum.

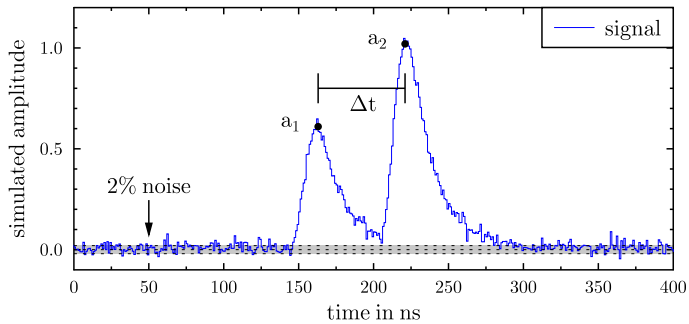

Figure 2.8: Simulated signal doublet with free parameters. Both amplitudes (a_1 and a_2), the signal distance Δt, and the noise level can be varied to test the algorithm.

Photon statistics

For very small signals it might be convenient to also study the effect of scintillation photon statistics. Because of the small amount of photons the simple exponential decay is no longer a valid model. Instead a base model is constructed by randomly generating photons and distributing them along the signal in an exponentially decaying fashion. This leads to the shapes shown in the left part of figure 2.7, which are made up of different amounts of photons N. It is obvious that for large N the signal approaches the exponential shape again. The use of photon statistics as the underlying model introduces a second source of uncertainty besides the noise amplitude to the signal. The magnitude of the uncertainty is of course correlated with the pulse amplitude, as is shown in the right part of figure 2.7. At the beginning of the pulse the uncertainty is minimal.

2.3.2 Determination of optimal trigger parameters

To determine the optimal trigger parameters a two step parameter scan has been conducted. During the first step the parameters governing triggering and timing (Trigger filter width t_{ftw} and Trigger threshold a_{thr}) have been investigated, while the second step covered the parameter for pile-up correction (Calorimetry filter width t_{fcw}). For each parameter set a test doublet of two signals was simulated. Figure 2.8 shows this situation with the free parameters (Amplitudes a_1, a_2, time difference Δt and noise level a_n). The trigger performance and the effectiveness of the pile-up correction algorithm was then investigated under variation of the test situation. To also get an idea of the statistics for each situation, each single parameter setting was benchmarked for a number of times. The following parameter scans have been carried out:

Scan Nr	Amplitude 1 [%]	Amplitude 2 [%]	t_{ftw} [ns]	t_{fcw} [ns]	Δt [ns]	SNR	a_{thr} [%]	N
1	[20,100]	100	[1,30]	1	[0,60]	[20,4]	[0.1,0.5]	20
2	[20,100]	100	[1,30]	1	[0,30]	[4,2]	[0.1,0.5]	20
3	100	[20,100]	[10,30]	1	[0,30]	[20,2]	[0.1,0.2]	20
4	100	[20,80]	8	[1,30]	[10,59]	[20,2]	0.1	40
5	[20,100]	100	8	[1,30]	[31,59]	[20,2]	0.1	40

Table 2.1: List of parameter scans. Expressions in square brackets are inclusive ranges. N is the number of iterations carried out for each setting. The signal to noise ratio (SNR) is only given for the smaller amplitude.

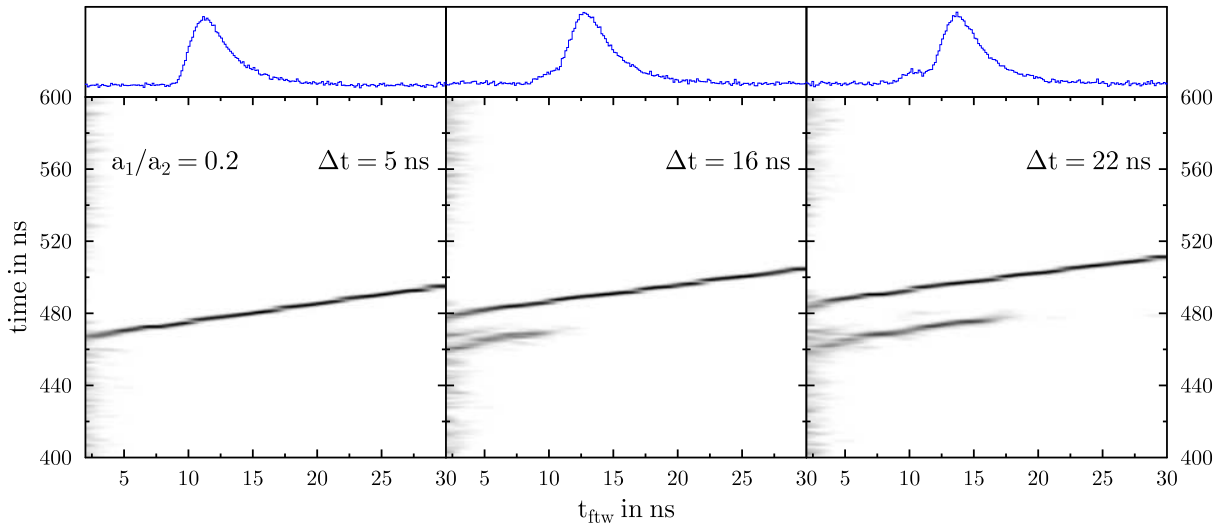

Figure 2.9: Density plot of parameter scan for a large signal following a small one with an amplitude ratio of $a_1/a_2 = 0.2$. From left to right the distance between the signals Δt is increasing. Each column in the density plot shows the probability of a trigger at a certain time step (vertical axis, zoomed in). The corresponding filter width t_{ftw} is drawn along the horizontal axis. The upward slope is due to the shift introduced by the filter.

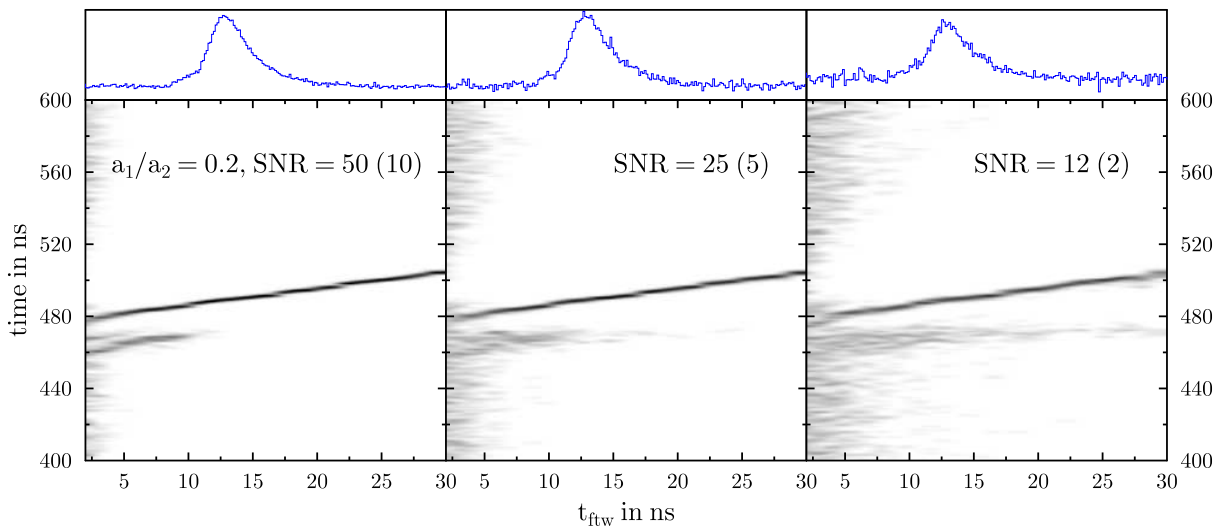

Figure 2.10: Results of parameter scan with a fixed value for $\Delta t = 16$. The noise level is varied to yield a decreasing signal to noise ratio (SNR) from left to right. The SNR for the smaller signal is given in brackets.

Dependance on t_{ftw}

Because of the multitude of possible parameter combinations only a few of them will be discussed in the following. Figure 2.9 shows trigger scan results for the case that a large signal follows a small signal ($a_1/a_2 = 0.2$) for several time

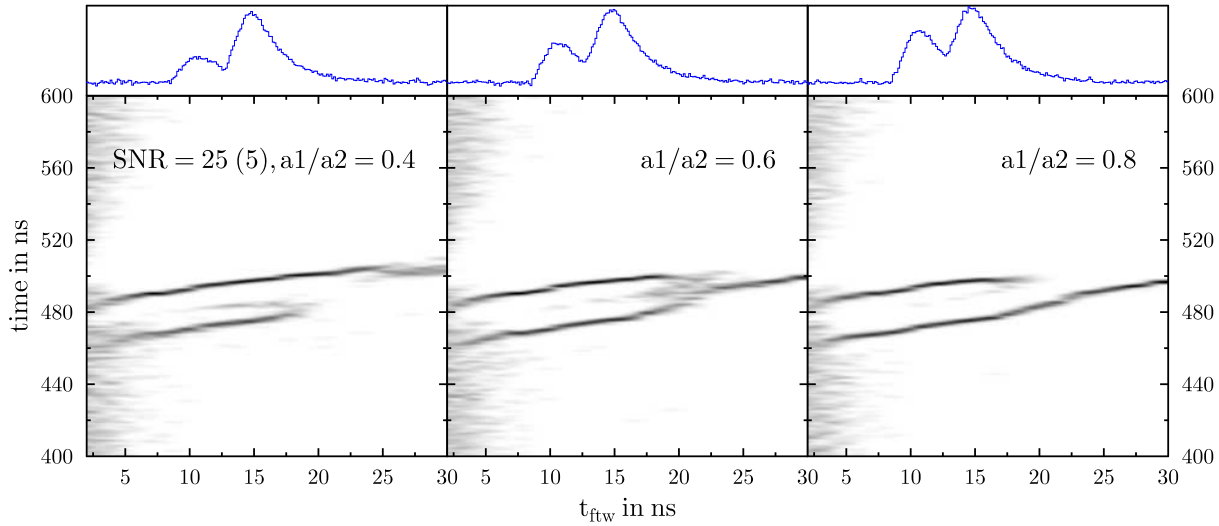

Figure 2.11: Results of parameter scan for varying amplitude ratio. From left to right the ratio increases while all other parameters are fixed. For large filter widths the behavior becomes unpredictable.

difference settings ($\Delta t = 5, 16, 22$ ns). The resulting data sets of scans 1 and 2 have been used. They contain trigger timing histograms for each parameter setting. These histograms are combined into two-dimensional density plots shown in figure 2.9 and the following figures. Along the horizontal axis the width of the timing filter (t_{ftw}) is plotted, while the vertical axis shows the trigger time. On top of each density plot the respective simulated signal is shown.

Obviously the trigger can distinguish both pulses only when they are a certain distance apart. The smallest distance for this case has been determined to be 16 ns, but for greater distances the trigger timing gets sharper. The best setting of t_{ftw} in this case is between 6 ns and 10 ns, because in this range two signals can be found. The figure also shows that, if the filter width is chosen too large, the second signal can not be found either. Thus it is advisable to choose t_{ftw} as low as possible, while still avoiding false triggering on noise for very low settings. In figure 2.10 the filter width is kept constant at 16 ns, but the Signal to Noise ratio (SNR) within the signals is varied. As expected, trigger precision is worse for higher noise levels. This degradation can not be recovered by increasing the filter width, because then the smaller signal can not be found. For detection of very small amplitudes it is thus very important to keep the noise level on the recorded signals at a minimum. In figure 2.11 the ratio of the two amplitudes is varied while keeping noise level and distance constant at $SNR = 25$ for the larger amplitude and $\Delta t = 22\,ns$. It can be seen that for a wider trigger filter width the trigger behavior is rather unpredictable and the trigger might not even find both signals. This is another reason to keep the filter width at a reasonable minimum. For the rest of the analysis and the determination of further parameters a fixed value for the filter width is set to 8 ns. This is about the length of the signal rise time.

Dependance on t_{fcw}

To determine an estimate for the optimum value for the calorimetry filter width t_{fcw} scans 4 and 5 have been performed. The filtered pulses have been fed into the pile-up correction algorithm. The reconstructed amplitudes are shown in figure 2.12 for various distances Δt and a fixed amplitude ratio of 0.8 as well as a fixed SNR of 40. On the horizontal axis the calorimetry filter width is varied. Only small differences can be seen for different distances, but as expected the amplitudes are better defined for greater distances. As for the timing filter width, it can be seen that for small time differences a smaller filter width is favorable, while for greater distances a wider filter width yields better results. This is due to the fact that larger integration intervals usually create a more stable amplitude. It is therefore possible to find an optimum value for the filter width somewhere in the middle. With increasing noise level, the amplitudes are less well defined, but for greater time distances the results tend to be better, as is shown in figure 2.13. In figure 2.14 the influence of the amplitude ratio is investigated and it is again clear that for values between 10 and 20 ns of the filter width the results show the sharpest distribution for all ratios. To sum it up, the best value for the calorimetry filter width depends on the distance of the following signal, but it should be chosen large enough to create a stable amplitude. For most cases a value of about 20 ns (2.5 times the rise time) is a good choice.

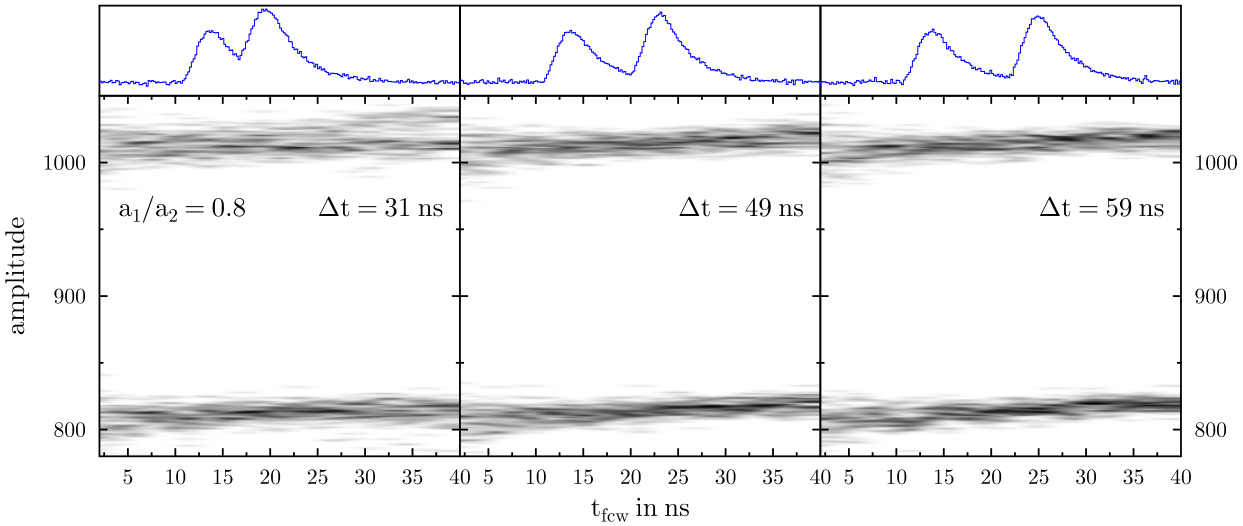

Figure 2.12: Results of parameter scan for various time differences. From left to right the difference increases. The best results can be found for medium values of t_{fcw} around 20 ns.

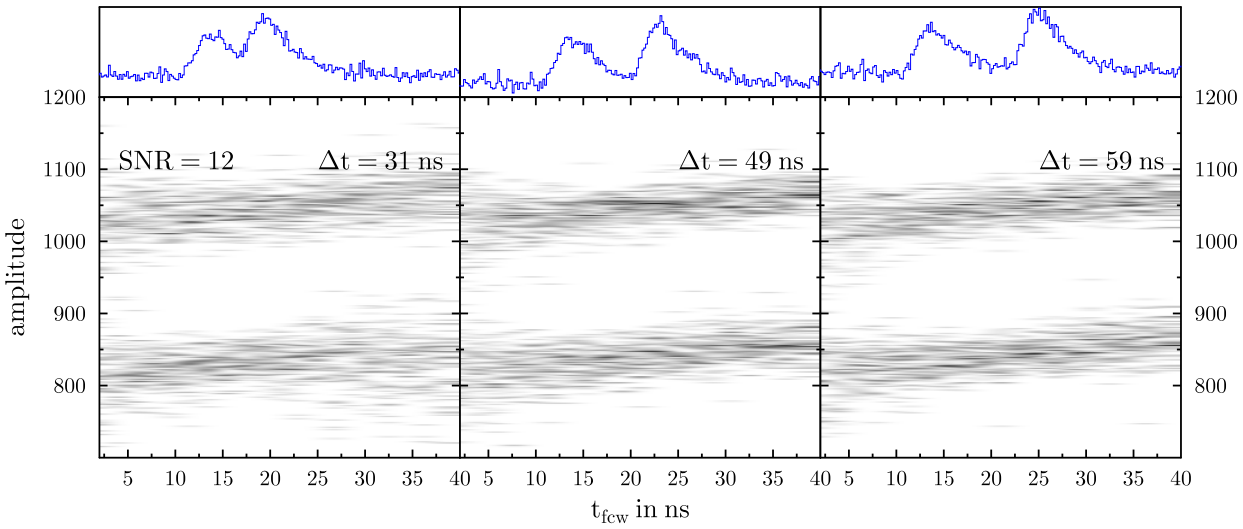

Figure 2.13: Results of parameter scan for larger noise level compared to figure 2.12. At this setting it is difficult to say which filter width t_{fcw} is favorable.

2.3.3 Effectiveness of pile-up correction

Now the effectiveness of the pile-up correction algorithm is tested. To keep this section short only the most difficult cases are shown here. These include extreme amplitude ratios, small SNRs and very small time distances.

For the following discussion the filter widths are set to fixed values ($t_{\mathrm{ftw}} = 8\,ns$, $t_{\mathrm{fcw}} = 22\,ns$). Figure 2.15 shows three different cases once without pile-up correction in the upper part and with pile-up correction applied in the lower part. The first case is the set up with a moderate amplitude ratio of 0.8 and also low noise. Without pile-up correction the first signal amplitude can be determined quite well to 0.8, but the second amplitude is strongly overestimated up to time differences of 50 ns. This would lead to serious pile-up artifacts in a spectrum. If instead the pile-up correction is applied to the amplitudes, then from time differences of about 20 ns on both amplitudes are correctly determined. For very small time differences there it is still the case that the sum of both amplitudes is determined. If spectroscopy is done on real data, then these really close signals should be rejected. The second case (middle pane of figure 2.15) demonstrates the pile-up correction for a signal doublet with a noise level ten times higher. The black region in the lower part of the plots is due to incorrect triggers on noise and should be overlooked. In this case there are no pulses with a comparably low amplitude. If the amplitudes are only measured, then again the amplitude of the second signal is overestimated,

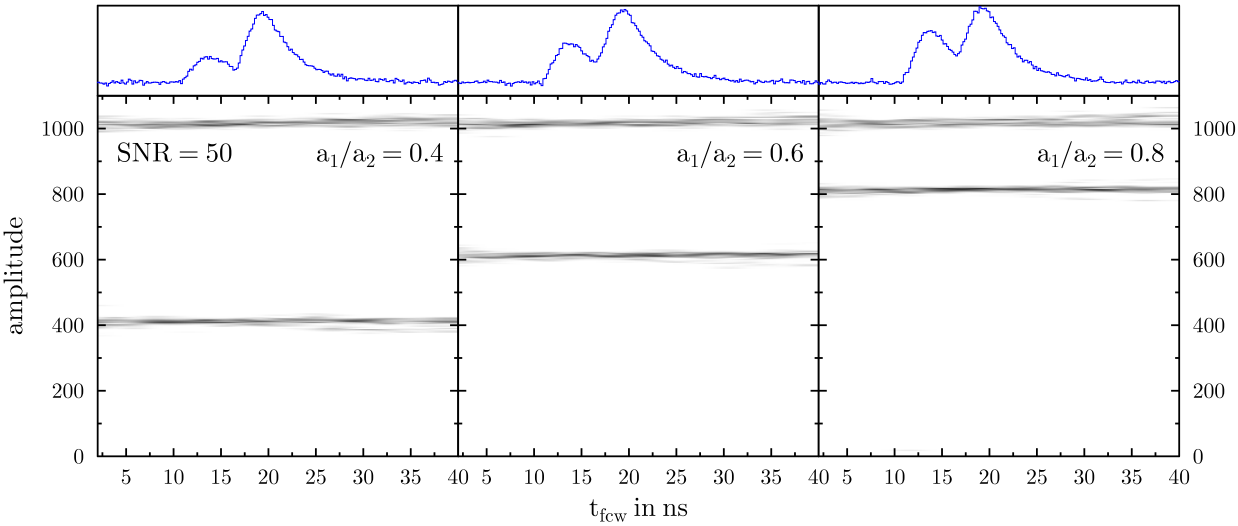

Figure 2.14: Results of parameter scan for various amplitude ratios. For all shown ratios a filter width t_{fcw} between 10 and 20 ns yields the best results.

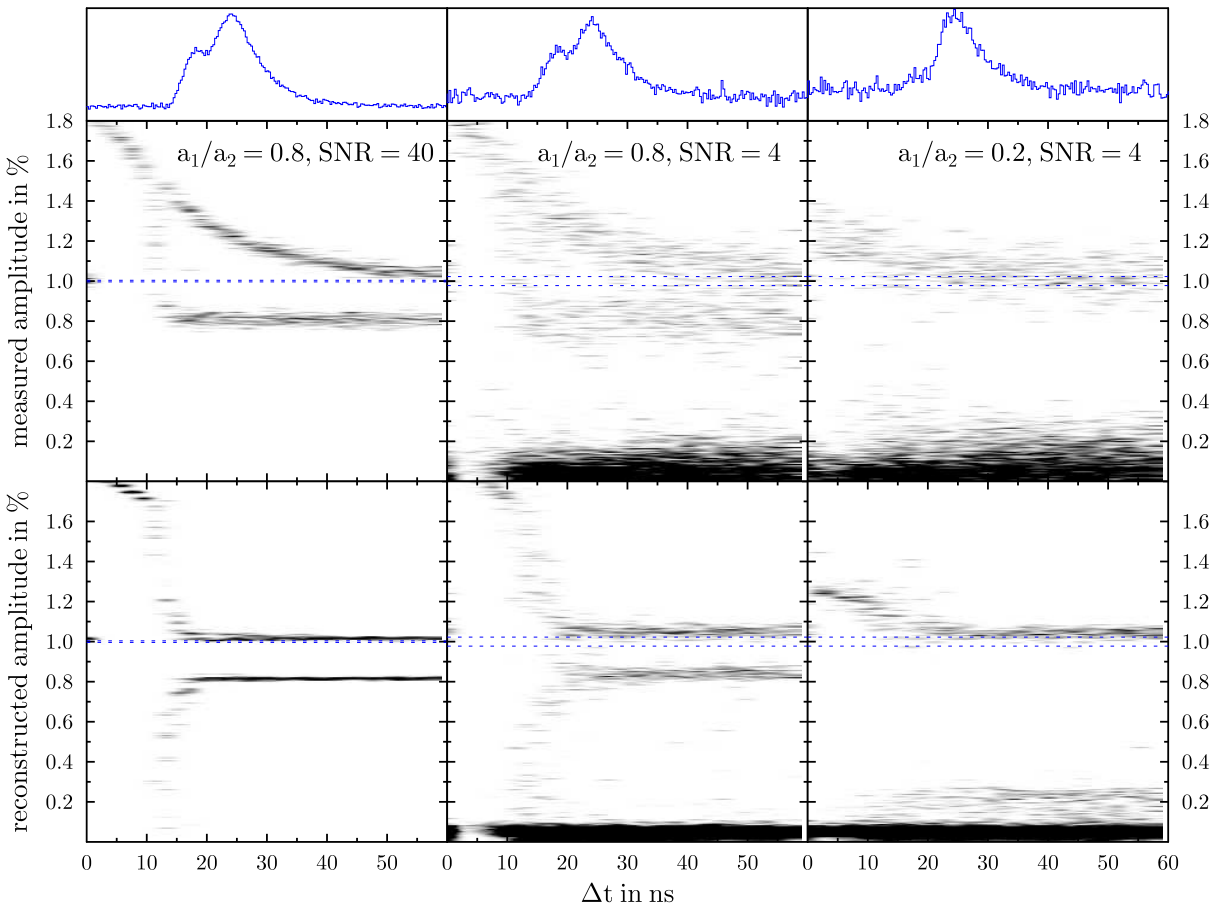

Figure 2.15: Scan results for measured (pile-up corrected) amplitudes are shown in the upper (lower) half plotted over the distance of the two signals. The dashed lines indicate the 1σ interval, if only one signal is present. Thus most of the uncertainty is due to noise and not a weakness of the algorithm.

and it is not as precisely determined. After pile-up correction the amplitudes are correctly restored with a much smaller

uncertainty as before. On the right the case is shown, where not only the noise level is high, but also the amplitude ratio is only 0.2, so the amount of information available is in this case at a minimum. This results in the amplitude of the first signal getting lost in the trigger noise. Note that the mean distortion of the second amplitude is not as high as in the previous cases, but this is only due to the fact that the first signal is much smaller in comparison. After pile-up correction the amplitudes are again restored and it is even possible to distinguish the amplitude of the first signal from the trigger noise. It is however not possible to cleanly restore the amplitudes of signals with a time difference well below 20 ns. Still the transition region between measuring the sum amplitude and the correct single amplitudes is rather narrow. To evaluate the amount of uncertainty introduced solely by the noise component, the dashed lines are shown in each plot. They indicate the 1σ interval around the mean value of the determined amplitude, if only a single signal is present. It is clear, that in the pile-up corrected cases the uncertainty is mostly due to the additional noise component.

Simulated traces

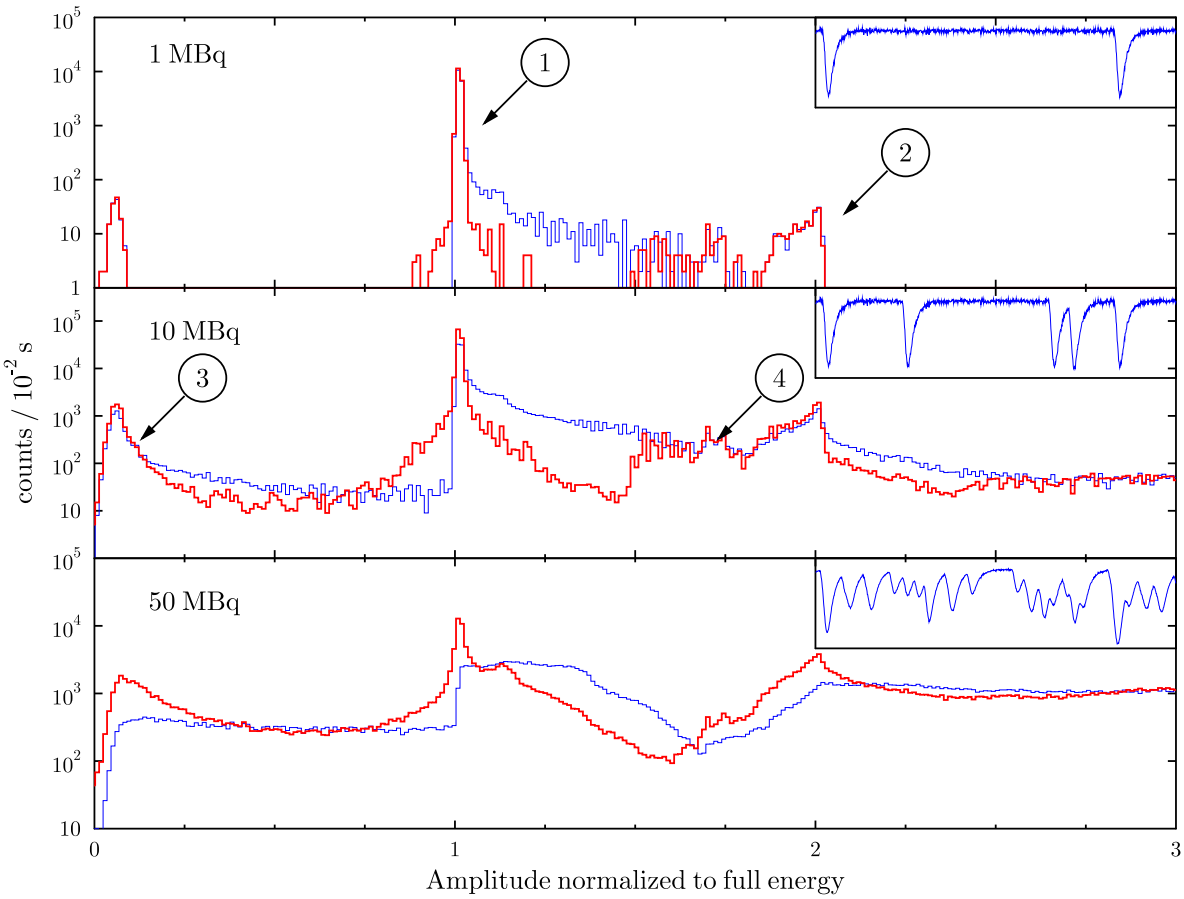

Figure 2.16: Spectra for simulated traces. In blue (red) spectrum with measured (pile-up corrected) amplitudes. The insets display portions of the simulated trace. *Top*: Simulated event rate at 1 MBq. The spectrum shows the full energy peak at ① and a summation peak at ②. *Middle*: 10 MBq, ③ Pedestal originating from triggering on noise, ④ Artifacts from limited trigger resolution. *Bottom*: 50 MBq.

In the next step long traces are simulated with randomly distributed model pulses. Each trace is 10^7 samples long which corresponds to 10^{-2} seconds. Using the previously determined optimum values for the filter widths the pile-up correction algorithm is applied to the simulated traces. The results can be seen in figure 2.16, where the measured amplitude spectrum is compared to the pile-up corrected spectrum and a spectrum simulated at low event rates. Several cases are shown.

At first the event rate was varied in between 1, 10 and 50 MBq corresponding to about $\frac{1}{60\tau}$, $\frac{1}{6\tau}$ and $\frac{1}{\tau}$. In the low rate spectrum the peak at amplitude 1 ('full energy', marked with ①) can be seen very clearly, and also the peak at twice the amplitude ② is visible. Pile-up artifacts have already been reduced from the right tail of the full energy peak. At the very

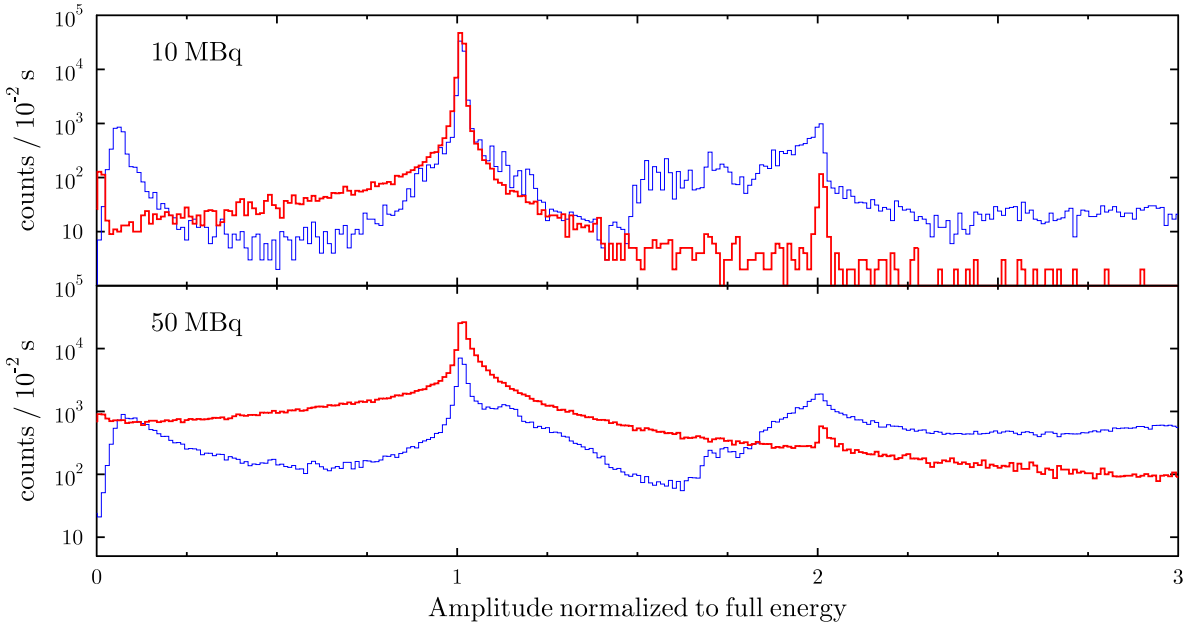

Figure 2.17: Spectra for simulated traces. In blue (red) spectrum with FIR trigger (original timestamps). *Top*: Simulated event rate at 10 MBq. *Bottom*: 50 MBq, for details refer to text.

low end of the spectrum a pedestal due to incorrect triggering on noise ③ is present. The photo peak efficiency (relative to the actual amount of signals in the input trace) within a 5 % interval is 90.2(7) % for the uncorrected and 95.8(7) % for the corrected spectrum, while the absolute efficiency is at 99 %.

At 10 MBq the difference between the corrected and uncorrected spectra is more noticeable. Pile-up artifacts in the uncorrected spectrum between full energy and the sum peak have increased a lot and also second-order pile-up effects beyond the sum peak are visible. With pile-up correction these artifacts are reduced by at least a factor of three for direct pile-up and a factor of two for second-order effects. Please note, that additional artifacts can not be corrected in the region just below the sum peak ④. This is due to the fact that signals which are too close together can not be separated with the trigger mechanism of the analysis. This is a fundamental limitation introduced by the trigger mechanism and can not be addressed by improving the pile-up correction algorithm. Further evidence for this hypothesis is that in a spectrum generated without a trigger mechanism, but instead using the original time stamps of the event generator, these artifacts do not show up. This is shown in the upper half of figure 2.17. The photo peak efficiency within a 5 % interval is 45.2(2) % for the uncorrected and 63.6(2) % for the corrected spectrum, while the absolute efficiency is at 86 %.

At a rate of 50 MBq (Fig. 2.16) the uncorrected spectrum completely lacks a defined full energy peak and shows almost no structure whatsoever. After pile-up correction the full energy peak as well as the sum peaks at twice and three times the full amplitude can be restored. To the right side of the full energy peak a small artifact from the summation of incorrect triggers and correct triggers is visible. The photo peak efficiency within a 5 % interval is 4.2(1) % for the uncorrected and 2.4(1) % for the corrected spectrum, while the absolute efficiency is at 35 %. If again the original time stamps are used, then all artifacts vanish from the pile-up corrected spectrum (Fig. 2.17, bottom).

As a second test for the algorithm simulated traces were produced for different noise levels corresponsing to SNR values of 50, 25, 12, 6, and 3. These traces have been simulated with an event rate of 10 MBq. The resulting spectra show a nice reconstruction of the full energy and the sum peak for SNR values of 50, 25, 12, and 6 (Fig. 2.18, top). Below this value the noise is too high for the trigger threshold and incorrect triggers distort the spectrum. A higher trigger threshold setting helps to reduce this effect, so that even very small signals can still be resolved (Fig. 2.18, middle). If the original time stamps are used, again the situation is improved and no artifacts are visible anymore (Fig. 2.18, bottom). In summary, pile-up correction using the matrix inversion algorithm works very well, but the results depend very strongly on the trigger mechanism. If signals are present, but no trigger pulse is generated, then the algorithm does not have the correct input data and consequently produces incorrect output.

A number of possible solutions are applicable and might help in this case. One approach would be to use pulse shape analysis to determine the rise time of each triggered pulse. If the rise time turns out to be too large, then disregard the signal, because a longer rise time indicates pile-up, or any other cause of signal distortion. Another solution would be

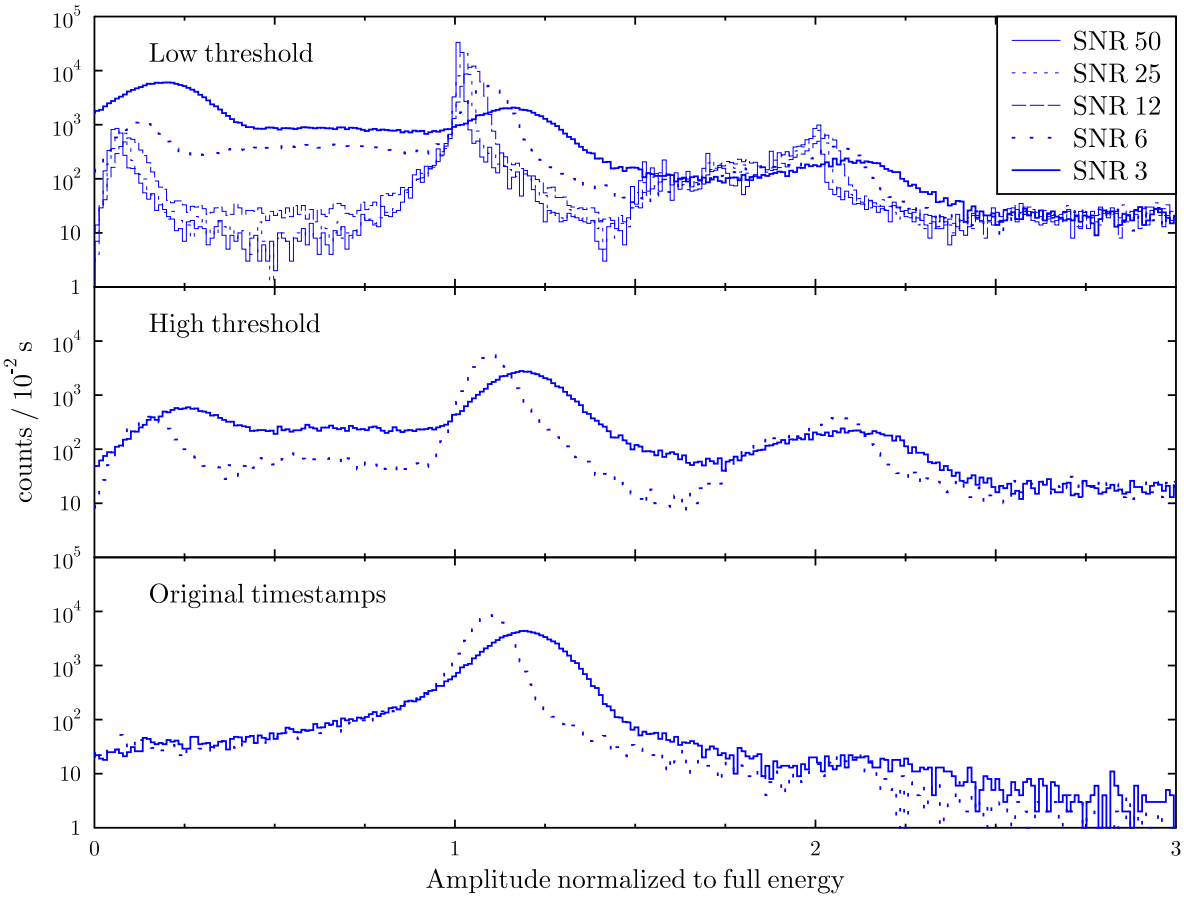

Figure 2.18: Spectra for simulated traces. *Top*: Spectra with different simulated signal to noise ratios. High SNR spectra (low noise) are drawn with thin lines. Low SNR spectra (greater noise) with thick lines. *Middle*: High SNR spectra gained with higher trigger threshold setting. *Bottom*: High SNR spectra with triggering on original timestamps.

to use several different trigger mechanisms, each one specially crafted to find either very small pulses, or pulses, which are very close together. A third approach would be an adaptive trigger mechanism, which would apply a simple forward deconvolution of the trace. The trigger would need knowledge of the pulse shape and can then subtract a pulse from the signal once it is found. This approach would also eliminate the problem of finding the baseline, because it would always stay at zero. Implementation of these algorithms is not part of this proposal, but can be considered for the Master's Thesis.

2.4 Application to measured traces

Since the actually planned detector has not been available so far, test measurements have been carried out with a smaller 0.5 by 0.5 inch scintillator, which was supplied by GSI.

2.4.1 Experimental setup

The experimental setup was done in a pretty simple way composed of just the lanthanum bromide detector and the radioactive sources. Several measurements were done, in which either the radioactive source was exchanged or the distance from the detector was varied in order to change the event rate. Data acquisition was done using a 2 GSample/s 8 bit *Tektronix* digital oscilloscope of type DPO7254. Data was taken with both a ^{60}Co and a ^{137}Cs source. Unfortunately the ^{60}Co source was not strong enough to deliver enough statistics in the amount of data recorded. One hundred traces, each with 2 million data samples have been taken.

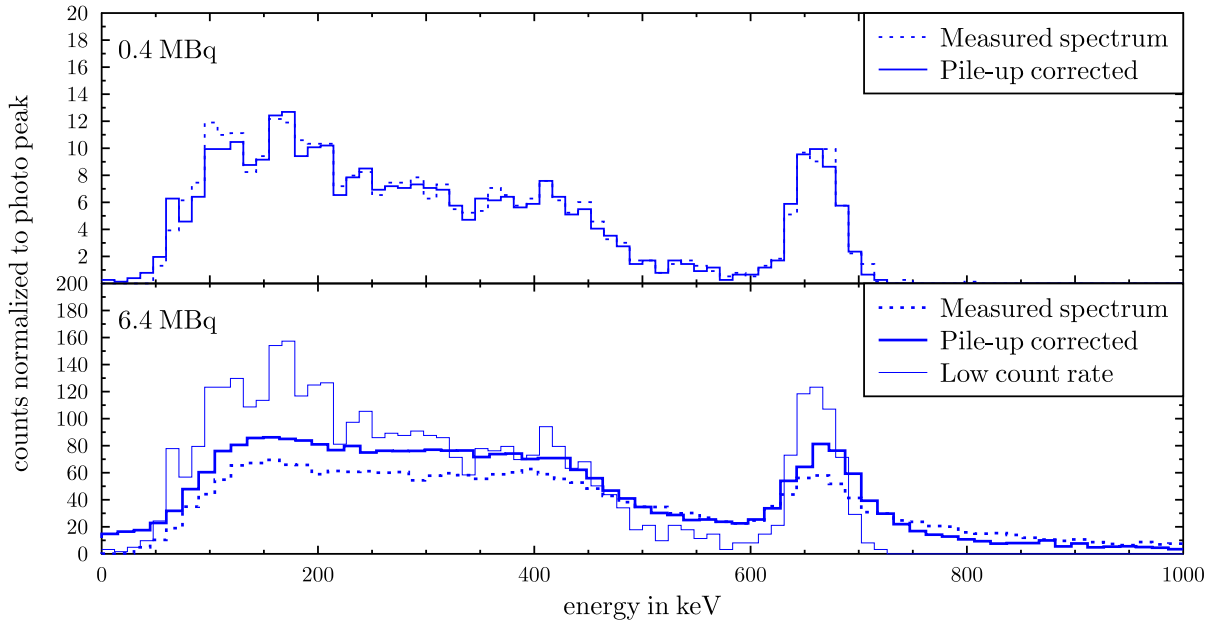

Figure 2.19: *Top*: Low count rate spectra of ^{137}Cs. Measured (pile-up corrected) spectrum drawn with dashed (solid) line. *Bottom*: High count rate spectra of ^{137}Cs (thick lines) in comparison to low count rate spectrum (thin line).

Low count rate

The upper part of figure 2.19 shows the results from the ^{137}Cs source at a distance of 87 cm. The spectrum contains about 26k events, which were recorded within 0.05 s. This equals an event rate of about 0.4 MBq. There is no noticeable difference between the recorded (dashed line) and pile-up corrected (solid line) spectrum, because the event rate is too low for pile-up to become important ($n\tau = 6 \cdot 10^{-3}$). The spectrum also contains only a few events to the right of the full energy peak, which is further evidence, that at this rate no significant pile-up occurs. The FWHM of the full energy peak is 46.3(2) keV in both cases.

High count rate

If the source is moved closer to the detector and measured at a distance of 23 cm, then the event rate increases by a factor of 16 to 6.4 MBq ($n\tau = 0.1$). The measured (dashed line) and pile-up corrected (thick line) spectra are shown in the lower part of figure 2.19 together with the measured spectrum at low count rate. The spectra are normalized to the number of counts in the full energy peak. Again the total recording time was 0.05 s, but the spectrum contains about 320k events. Pile-up correction clearly helps restoring photo peak efficiency and resolution of the spectrum at high count rates. The peak to total and FWHM values are 7.9(3) % and 79.0(3) keV for the measured spectrum and 9.8(2) % and 69.9(2) keV for the pile-up corrected spectrum. Pile-up events in the high energy tail have been reduced from 12.4 % to 6.3 %, which is a reduction of about 50 %. This shows that pile-up correction can be done on realistic data sets with the used method.

Discussion

From the lower part of figure 2.19 it is clear that also a great deal of pile-up events have not been restored with the applied algorithm. This is largely due to the fact that the trigger component is rather simple, as already discussed in paragraph 2.3.3. To improve this situation, the trigger is the first component that has to be reviewed and extended. Since triggering and timing is the crucial part of the analysis, it is very important to develop a stable and extremely sensitive, but noise-resistant trigger and timing method.

3 Tools

In this chapter I want to outline the design goals for the acquisition software and some of the features of the DSP library *SamDSP*, written in C++. For data acquisition and analysis I have developed a set of tools, which is supposed to fulfill two main objectives. At first the interface between PC and ADC hardware should be easy to handle and also enable simple setup and data acquisition. It should also be possible to monitor the acquired data directly to make corrections to the setup and configuration. The second important objective is to create a base library that serves as a toolbox providing powerful digital signal processing methods.

3.1 Software Scope

3.1.1 Version history

The main goal of the software started out as to simply be able to configure the Flash ADC, acquire the recorded data and write the traces to disk. The first version was just a command line based read-out tool with no visual feedback, merely extending the Struck examples to file output. It was possible to record traces, but only if the hardware configuration had been correctly determined using a separate tool, which did not allow data storage. The next version featured a graphical user interface (GUI) with control buttons and a scope-like window, where the acquired traces were displayed upon acquisition. This way the correct parameters could be determined and set up within a single application. The design was still very strict and only allowed to access the SIS3350 ADC [SIS08d] via the SIS3150usb [SIS08c] USB interface. In the course of development it became clear that it would make sense to shift the scope of the application a bit and allow more flexibility.

3.1.2 Current state

Currently the application is structured in a modular way which uses two C++ classes for each VME module. One class provides the user interface layout for parameter controls and setup, the other class provides the necessary VME calls. Both classes can be accessed using a general interface independent of the VME module that is being configured. Due to this modular approach it will be easy to write additional classes to support more VME modules in the future. In the current state the scope software can use either the SIS3150usb USB interface or the SIS3100 PCI-Express interface [SIS08b] to access the VME modules. It is possible to record data with the 4 channel 500 MHz flash ADC SIS3350 and the 8 channel 100 MHz SIS3302 flash ADC [SIS08a]. Another great feature that has a lot of potential is the post processing option. Any data that has been read out from any module can be rerouted to pass a through a post processor class. Within this class arbitrary signal processing or logical operations such as digital filtering or coincidence checking can be applied to the data. Any step in this process can be visualized in a graph window. Currently it is possible to directly record an amplitude spectrum of the acquired traces and display it on the screen. This has been implemented in order to be able to check and correct the input gain parameters of the FADC. The post processing class makes heavy use of the DSP methods provided by the *SamDSP* library.

3.2 DSP library SamDSP

The development of the *SamDSP* library began as a C++ conversion of Matlab methods for the pile-up correction algorithm to improve the computing speed. It is based on the C++ Standard Template Library (STL) [SGI94] and makes extensive use of the vector container class and some of the supplied algorithms. For some methods also the GNU Scientific Library (GSL) [GSL08] is used. In the process of the development a lot of functions for vector and matrix calculation and manipulation have been implemented. Signal processing functions such as filter and convolution methods and a range of different digital trigger methods are available. Powerful generic algorithms such as the ISODATA Fuzzy C-Means [Dun73] clustering algorithm or the pile-up correction algorithm for fast detector signals are part of the library. Another set of functions is specifically written to provide high speed calculations with a minimum of overhead.

3.2.1 List of methods

Vector manipulation functions

max, min	Minimum and maximum value
add, addC, sub, mul, div, scale, rscale, scalar	Simple arithmetic manipulations
shift, rotate, pad	Rearrange vector elements
integrate	Return integrated vector
average	Vector average
distance	Euclidean distance of two vectors
histVector	Make histogram from vector

Matrix manipulation

identity	Generate identity matrix
gslSvdInverse	Computes inverse of matrix
projectRows	Horizontal projection of matrix
projectColumns	Vertical projection of matrix

Filter kernel generators

boxkernel	Generate the respective kernel
biboxkernel	
rampdownkernel	
mwdkernel	
poissonkernel	
sinckernel	
range	Return an integer range

Simulated signals

prototypePMT	Generate exponential signal
prototypeTrace	Generate trace with randomly distributed signals
statisticsScint	Generate signal from photon statistics
createNoise	Generate noise signal

DSP

triggerLET	Leading edge trigger
triggerLMT	Local maximum trigger
triggerTET	Trailing edge trigger
triggerCFD	Digital constant fraction trigger
triggerACFD	'Analog' constant fraction trigger
phasesCFD	Compute 'phase' of trigger time
resample	Resample signals to change sampling rate
restoreBaseline	Automatically restore the baseline
fcm	ISODATA fuzzy c-means cluster algorithm
unpile	Pile-up correction algorithm

Optimized algorithms

So far some filtering methods and vector operations have been implemented again to optimize for speed. A speed-up of a factor of 30 has been achieved in some cases.

Output functions

vectorPrint	Console output
matrixPrint	
vectorToFile	File output
matrixToFile	

4 Outline for the Master Thesis

4.1 New 3x3 inch detector

So far the pile-up correction method has mostly been applied to artificial signals, and a rigorous test with real detector has not been conducted yet. In November 2009 a new 3 by 3 inch LaBr scintillation detector has been ordered from Canberra [CAN10], which is to be delivered in May 2010. This detector will at first be used for further tests of the pile-up correction algorithm, while its final purpose is to serve as an active beam dump at the photon tagger NEPTUN. Similar to the investigation of effects of different parameter values for simulated pulses, as shown in this proposal, the influence of the parameters will be studied undet different conditions. The main goal is to investigate the effectiveness of the method when applied to real signals, and to identify its limits. Throughout this proposal it has been stated several times, that the performance of the used trigger method is of great importance, and that the pile-up correction quality strongly depends on the choice of the trigger method. Thus the second most important goal is the development and test of different trigger methods. The perfect method would be one that is able to detect every pulse with high accuracy. In detail the following points will be addressed during the Master Thesis:

Test with radioactive sources

To determine the basic properties of the new detector, measurements with a range of radoactive souces will be conducted. For this purpose the *Institut für Kernphysik* has high activity ^{137}Cs and ^{60}Co sources available. It might be interesting to also have a strong source with a lower energy, such as ^{57}Co or ^{133}Ba available.

Test with an X-Ray tube

The very high photon flux at energies in the range of 30 to 140 keV emitted from an X-Ray tube is an excellent environment to investigate with the new detector. Since St. Gobain attested best detector performance only at energies above 100 keV, it is an interesting challange to see, if this limit can be lowered using digital techniques. Another interesting point would be to investigate the effectiveness of absorbers for low energy X-rays, because these events are usually of limited value, but contribute to the total count rate and thus decrease trigger performance. This can be done with an X-ray tube and a radioactive source with a higher energy. The X-rays can be screened with a range of different absorber materials, while measuring the energy resolution of the emitted γ-rays from the radioactive source. The results of this investigation can be used for the design of the beam dump.

Impact of PMT voltage

In very high count rate measurements the signal amplitude of the PMT output decreases with increasing detection rate, because of space charge effects in between the PMT dynodes and also depletion of dynode capacitors. Adjusting the PMT voltage can have positive effects to counteract this condition as is discussed in [HAM07]. The response of the new detector to PMT voltage adjustment will be tested.

Setup and test of an active beam dump

Since it is planned to install the detector as an active beam dump, the design and construction of the setup has to be carried out. The design goals are to enable the experimentalist to measure the tagged beam energy and photon flux. Background shielding and suppression of scattered photons should be taken into account in the design. A graded shield design using copper to suppress low energy It may be necessary to collimate the beam in high current experiments, so easy collimation adjustment should be possible.

Integration with current data acquisition

In order to have a single interface to the data acquisition hardware, the new detector should be integrated into the current acquisition system as much as possible. This procedure is challanging since the current system is completely comprised of analog VME modules. The addition of a digital readout and processing section might prove difficult to be implemented in the current software. The most prominent problem in coping with digital hardware is the high data bandwidth and processing power that is necessary to handle the recorded data. One idea is to use a standard multi-core PC to take care of both analog and digital readout, instead of the limited single-slot PC within the VME crate. Some remarks on how this could be realised are drafted in the next section.

4.2 Extension of the Scope and SamDSP

In the future I would like to extend the number of VME modules that can be controlled and read out with the software. It is necessary to be able to collect data from analog modules like the ones from CAEN which we currently have in operation at NEPTUN. The integration of these modules would allow to mix digital and analog data acquisition and provide a common platform. The second most important future development is to split the post processing class into many small plugins with their own inputs and outputs which can be interconnected and share their data. The goal here is to create a modular framework that allows to define for each data input stream from each VME module a path through the post processor to allow online data analysis with a high degree of flexibility without sacrificing acquisition speed. For instance the amplitude spectrum plugin would take traces from the FADC as input, calculate the amplitudes and then send the updated spectrum as output to the file output plugin. Alternatively there could be a network output plugin or a plugin for a *root* [Roo10] framework interface.

During this development it has to be kept in mind that currently all steps of the acquisition, processing, data display and data storage process are done sequentially. This implies that the next acquisition can only take place after the last stage of processing is finished, which reduces acquisition speed significantly. The solution is to allow time consuming parts of the process, i.e. file output or large calculations, to be executed in parallel using separate threads. This approach would take advantage of the fact that modern PCs are usually equipped with more than one CPU and thus a threaded design would improve the application speed.

So far data acquisition has been conducted using a polling mechanism, which continuously tested the module of interest, if new data was available. This passive method is inefficient and increases the average system latency. An improvement is expected from moving to interrupt based data acquisition. In this case the module of interest issues a signal by itself, whenever new data is ready to be read out. This is already done in many other experiments and should should improve acquisition latency.

Useful extensions to the *SamDSP* library would be an interface to the *root* framework, making use of fast fourier transform methods from the FFTW package, and also least-squares fitting functionality. It would be very useful to also implement a baseline-follower algorithm, which keeps track of the baseline level over the course of very long traces. Also an extension of the trigger algorithm section in the form of an adaptive trigger, which takes into account the signal shape or dynamic would be of use. Finally incorporating the Kalman filter pile-up correction approach used for high count rate HPGe signals would widen the field of application for the library.

4.3 Hardware accelerated data processing

The advantage of moving parts of the data acquisition or the digital processing workload to specialized hardware is in most cases the great potential for speeding up the processing or in other cases to improve the latency of the setup. The cost is often that the implementation is more difficult due to the nature of the hardware. Also debugging of software proves much more difficult, because in most cases no basic input or output device like a terminal is available. Using current technology there are three main approaches to accelerate data processing: Special CPUs for digital signal processing (DSPs), field programmable gate arrays (FPGAs), or graphics processing units (GPUs) on standard graphics cards. In this case it is technically possible to try any of the methods, because the required hardware is available.

The SIS3350usb USB interface is equipped with two high power DSP units which could be programmed so that all data acquisition and event packing could be done within the VME crate without using a dedicated single-slot PC. Data acquisition would be reduced to setting up the DSPs correctly and reading the readily packed events from memory.

Most of the VME modules in our experimental setup are completely driven by FPGAs. In the case of the flash ADCs it would make sense to extend the current standard firmware to allow sophisticated digital signal processing methods to be applied to the recorded data directly after acquisition. The goal would be to reduce the data on the chip far enough to output only spectra and listmode data. This would for example enable real-time spectrometry with very high rates or digital pulse shape identification using only one flash ADC.

The last method of moving processing tasks to the GPU is always feasible, when the same operations have to be carried out on a large array of data simultaneously. For instance multiplication of large matrices can be done in a very efficient way. In digital signal processing operations like digital filtering or Fast Fourier Transformations can significantly be accelerated on the GPU. It might be reasonable to reimplement some of the methods in the *SamDSP* library, so that they can be moved to the GPU. One has to take into account the additional overhead introduced by the fact that the necessary data have to be copied to and from the GPU before and after processing.

4.4 Roadmap

In this last section I am going to try putting the various future tasks in a reasonable chronological order.

Nr	Task	Duration	Importance
1	**Test of new detector**		
1.1	Test with radioactive sources	3 w	++
1.1a	Purchase of new source	(1 w)	o
1.2	Test with an X-ray tube	(1-2 w)	o
1.3	Impact of PMT voltage	1 w	++
1.4	Integration with DAQ	2 w	+
2	**Setup and test of active beam dump**		
2.1	Design	2-3 w	++
2.2	Construction	4 w	++
2.3	Commissioning without beam	1 w	++
2.4	Commissioning with beam	–	++
3	**Software improvement**		
3.1	Extension of scope software	1 m	++
3.2	Extension of *SamDSP*	1 m	++
3.3	Test of Hardware accelerated DSP	(1 m)	o

Table 4.1: List of future tasks with expected duration and importance rating.

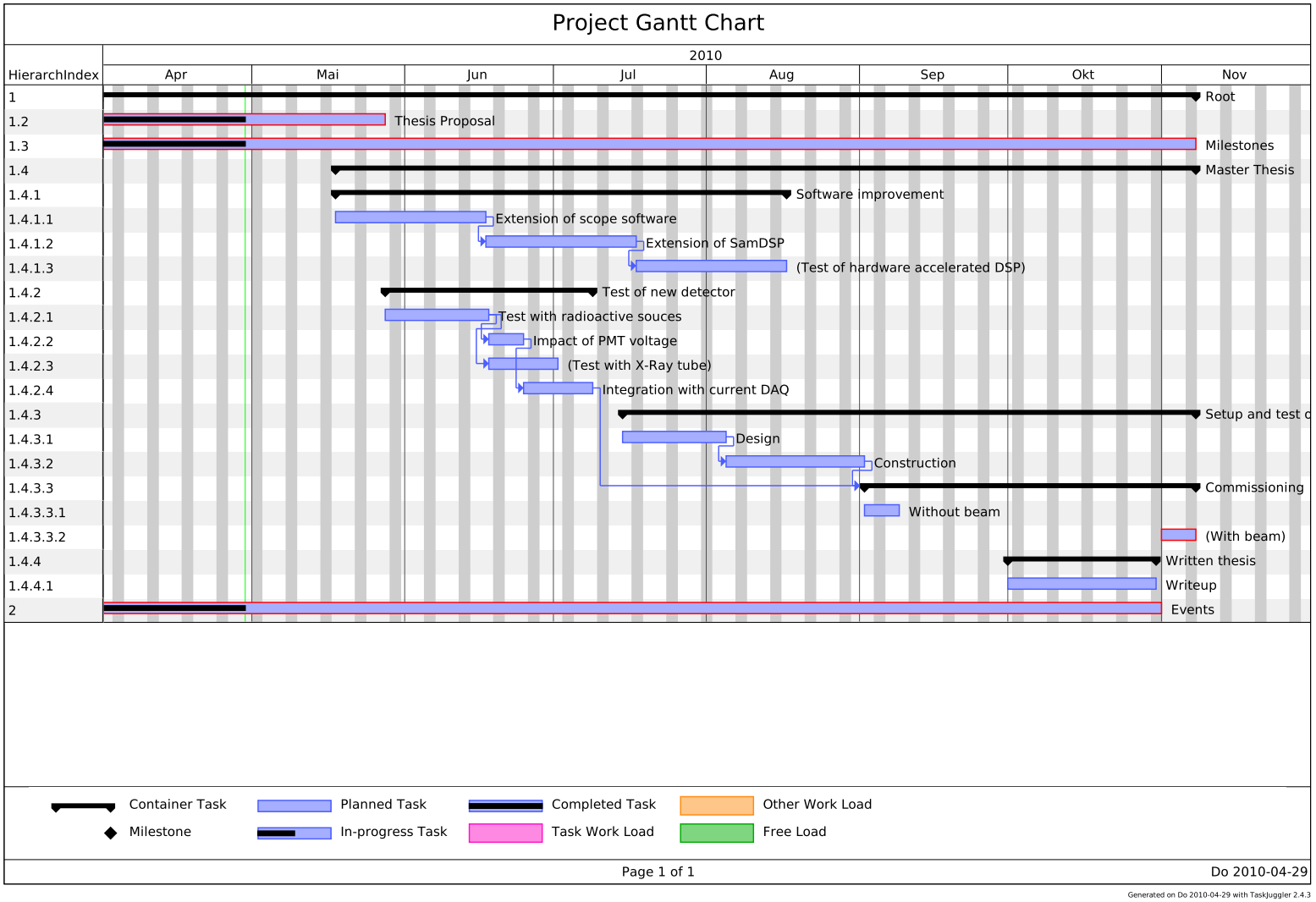

Figure 4.1: Gantt chart of future work units.

List of Tables

List of Figures

Bibliography

[Bar06] É. Barat, T. Dautremer, T. Montagu, J.-C. Trama, Nuclear Instruments and Methods in Physics Research A **567** (2006) 350.

[Bel08] F. Belli, B. Esposito, D. Marocco, M. Riva, Y. Kaschuck, G. Bonheure, J. E. Contributors, Nuclear Instruments and Methods in Physics Research A **595** (2008) 512.

[Ben74] B. Bengtson, M. Moszynski, Nuclear Instruments and Methods **117** (1974) 227.

[Ben78] B. Bengtson, M. Moszynski, Nuclear Instruments and Methods **155** (1978) 221.

[CAN10] *CANBERRA GmbH Home Page*, http://www.canberra.com/de/ (2010).

[Dun73] J. C. Dunn, Journal of Cybernetics **3** (1973) 32.

[Geo93] A. Georgiev, W. Gast, IEEE Transactions on Nuclear Science **40** (1993) 770.

[GSL08] *GNU Scientific Library Online Documentation*, http://www.gnu.org/software/gsl/manual/html_node/ (2008).

[HAM07] *Hamamatsu Photonics K. K., Photon is our Business*, self-published, 3rd Edition (2007).

[Kno00] G. F. Knoll, *Radiation Detection and Measurement*, John Wiley and Sons, Inc, New York, 3rd Edition (2000).

[Men06] P. R. Menge, *Performance of large BrilLanCe 380 (lanthanum bromide) scintillators*, Presented at SORMA XI, Ann Arbor MI (2006).

[Ric96] A. Richter, Proc. 5 EPAC, Eds. S. Myers et al., IOP Publishing, Bristol (1996), 110.

[Roo10] *ROOT Framework Home Page*, http://root.cern.ch/ (2010).

[Sav10] D. Savran, K. Lindenberg, J. Glorius, B. Löher, S. Müller, N. Pietralla, L. Schnorrenberger, V. Simon, K. Sonnabend, C. Wälzlein, M. Elvers, J. Endres, J. Hasper, A. Zilges, Nuclear Instruments and Methods in Physics Research A **613** (2010) 232.

[SGI94] SGI, *Standard Template Library Programmer's Guide*, http://www.sgi.com/tech/stl/ (1994).

[SIS08a] SIS, Struck Innovative Systeme GmbH, *Datenblatt SIS3002*, http://www.struck.de/sis3002.htm (2008).

[SIS08b] SIS, Struck Innovative Systeme GmbH, *Datenblatt SIS3100*, http://www.struck.de/sis3100.htm (2008).

[SIS08c] SIS, Struck Innovative Systeme GmbH, *Datenblatt SIS3150usb*, http://www.struck.de/sis3150usb.htm (2008).

[SIS08d] SIS, Struck Innovative Systeme GmbH, *Datenblatt SIS3350*, http://www.struck.de/sis3350.htm (2008).

[StG08] Saint-Gobain Crystals, France, Data sheet of material BrilLanCe 380 (2008).

[StG09] Saint-Gobain Crystals, France, BrilLanCe Scintillators Performance Summary (2009).

[Ven09] M. Vencelj, K. Bučar, R. Novak, H. J. Wörtche, Nuclear Instruments and Methods in Physics Research A **607** (2009) 581.

[Yan09] H. Yang, D. K. Wehe, D. M. Bartels, Nuclear Instruments and Methods in Physics Research A **598** (2009) 779.

Erklärung zum Project-Proposal

Hiermit versichere ich, das vorliegende Project-Proposal ohne Hilfe Dritter nur mit den angegebenen Quellen und Hilfsmitteln angefertigt zu haben. Alle Stellen, die aus Quellen entnommen wurden, sind als solche kenntlich gemacht. Diese Arbeit hat in gleicher oder ähnlicher Form noch keiner Prüfungsbehörde vorgelegen.

Darmstadt, den 14. Mai 2010

(Bastian Löher)